

Climate Impact of Late Quaternary Equatorial Pacific Sea Surface Temperature Variations

David W. Lea,^{1*} Dorothy K. Pak,¹ Howard J. Spero²

Magnesium/calcium data from planktonic foraminifera in equatorial Pacific sediment cores demonstrate that tropical Pacific sea surface temperatures (SSTs) were $2.8^\circ \pm 0.7^\circ\text{C}$ colder than the present at the last glacial maximum. Glacial-interglacial temperature differences as great as 5°C are observed over the last 450 thousand years. Changes in SST coincide with changes in Antarctic air temperature and precede changes in continental ice volume by about 3 thousand years, suggesting that tropical cooling played a major role in driving ice-age climate. Comparison of SST estimates from eastern and western sites indicates that the equatorial Pacific zonal SST gradient was similar or somewhat larger during glacial episodes. Extraction of a salinity proxy from the magnesium/calcium and oxygen isotope data indicates that transport of water vapor into the western Pacific was enhanced during glacial episodes.

The equatorial Pacific ocean dominates the tropical ocean due to its size, because (i) it encompasses the warmest region of the oceans, the western Pacific warm pool; (ii) it is the principal source of water vapor to the atmosphere; and (iii) it influences interannual oscillations in climate (1). Previous studies of tropical sea surface temperature (SST) changes on glacial-interglacial time scales in the Pacific have been ambiguous. Results for the Pacific from CLIMAP (Climate: Long-Range Investigation, Mapping, and Prediction) obtained using faunal transfer functions indicate an area-averaged (20°S and 20°N) last glacial maximum (LGM) August SST that is $-1^\circ \pm 2^\circ\text{C}$, relative to the Holocene (2). Some studies using revised faunal methods support up to 2°C or greater cooling than originally suggested by CLIMAP (3), and results from alkenone unsaturation ratio data suggest cooling of 2° to 3°C (4, 5). In sharp contrast to all these studies are the inferences based on coral Sr/Ca, which suggest cooling of 6°C (6). The more extreme marine cooling estimates appear to be supported by terrestrial evidence, including a snow line lowering of 800 ± 50 m (7), noble gas records in ground waters (8), and isotope records from tropical alpine glaciers (9). Because of these conflicting data, the role of the tropical Pacific in driving glacial-interglacial climate change remains unresolved.

The Mg content of planktonic foraminifer shells is a proxy of past SST that has recently

been validated in a number of oceanographic settings (10–13). Mg paleothermometry has certain unique advantages over other proxies, the most important of which is that Mg/Ca is measured in foraminifer shells, which are by themselves a vital archive of past climate and the carrier phase for oxygen isotopes. Measuring both Mg/Ca and $\delta^{18}\text{O}$ in foraminifer shells from a deep sea core makes it possible to separate the magnitude and timing of SST and $\delta^{18}\text{O}_{\text{water}}$ changes (11, 13). The conundrum of tropical Pacific cooling is an ideal problem for the application of Mg paleothermometry, because this method can be applied to oligotrophic regions such as the western equatorial Pacific (WEP), where sediments contain insufficient organic carbon for application of the

alkenone unsaturation ratio technique.

We apply Mg paleothermometry in combination with coincident $\delta^{18}\text{O}$ measurements to determine the thermal and hydrographic history of tropical Pacific surface waters. We selected tropical sites that represent the two end members of the equatorial Pacific: cores from the Cocos Ridge and Galapagos Platform just north of the cold upwelling environment of the eastern equatorial Pacific (EEP), and a site on the Ontong Java Plateau (OJP) in the center of the Pacific warm pool (Fig. 1 and Table 1). We focus on tropical spinose planktonic foraminifera that directly represent sea surface conditions because they dwell in the mixed layer.

Temperature calibrations for Mg/Ca and influence of preservation. Several planktonic species have been calibrated for Mg uptake using core-tops and culturing (11, 13–15). These calibrations indicate that the Mg content of foraminifer shells is an exponential function of temperature with an increase of $9 \pm 1\%$ in Mg/Ca per $^\circ\text{C}$. The absolute Mg/Ca of the shells at a given temperature appears to be species-specific, necessitating individual calibration of each species. For temperature conversion in this study, we use a *Globigerinoides ruber* calibration based on core-tops from the tropical Pacific, which yields the following relationship (Fig. 2A) (16, 17): $\text{Mg/Ca (mmol/mol)} = 0.30\exp[0.089 \times \text{SST (}^\circ\text{C)}]$. The standard error of this fit is $\pm 0.6^\circ\text{C}$. For comparison, a published culturing calibration (14) for *G. sacculifer* yielded $\text{Mg/Ca (mmol/mol)} = 0.39\exp[0.089 \times T (^\circ\text{C})]$. These relationships have identical exponential terms and differ only in the pre-exponential constant. We hypothesize that the constant offset does not reflect uptake differences but rather a combination of the effect of a small addition of gametogenic calcite at colder temperatures and/or poorer

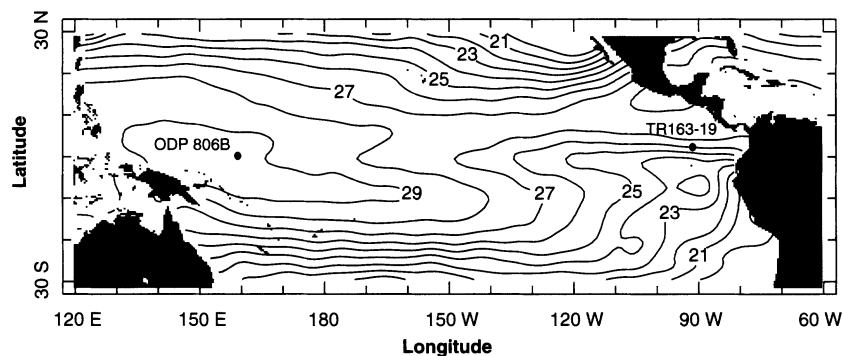


Fig. 1. SSTs in the tropical Pacific (43). The locations of the two principal cores in this study are indicated. Cocos Ridge core TR163-19 is located just north of the cold upwelling water that characterizes the EEP. Mixed layer thickness averages about 20 m with a relatively shallow thermocline in which temperature drops from 25° to 15°C within 100 m of the surface. Seasonal SST variation is about 3°C at the two more northeasterly sites (TR163-18 and TR163-19) and rises to 4°C at the two southwesterly sites (TR163-20B and TR163-22). ODP Hole 806B on the Ontong Java Plateau lies in the center of the western Pacific warm pool, the warmest ($>29^\circ\text{C}$) water mass in the oceans. This site is characterized by an 80-m-thick mixed layer ($T > 28^\circ\text{C}$) underlain by a deep thermocline in which temperature barely drops to 27°C at 100 m water depth. Seasonal variation is minimal, typically less than 1°C .

¹Department of Geological Sciences and Marine Science Institute, University of California, Santa Barbara, CA 93106, USA. ²Department of Geology, University of California, Davis, CA 95616, USA.

*To whom correspondence should be addressed. E-mail: lea@geol.ucsb.edu

preservation in core-top relative to cultured samples (18). To ensure that samples have experienced similar degrees of preservation, we restricted the core-top calibration to Pacific samples.

Because dissolution influences shell Mg/Ca, we measured Mg/Ca in *G. ruber* in a core-top transect on the OJP (Fig. 2B). These results indicate that Mg/Ca is biased to lower values (i.e., colder temperatures), at deeper depths, as has been previously demonstrated (18). This influence comes about either through the selective loss of shells formed in warmer water or through the selective loss of ontogenetic shell material enriched in Mg/Ca. Because surface water temperatures are so uniform in both time and space in the WEP, we favor the latter explanation. Our results demonstrate that shell Mg/Ca decreases by 0.6 mmol/mol for each kilometer of water depth, equivalent to a 12% drop per kilometer or a paleotemperature colder by about 1.3°C. Because all the cores consid-

ered here lie between 2030 and 3200 m depth in the equatorial Pacific, it is likely that they have experienced similar preservation histories. We calculate the potential influence of downcore variations in preservation (19, 20) to be equivalent to a +0.5°C bias in glacial paleotemperature estimation (21).

Eastern boundary current results from the Cocos Ridge and Galapagos Platform.

The oxygen isotope record from Cocos Ridge core TR163-19 reveals that it covers three full glacial cycles and that the deepest part of the core (10.5 m) ends in the latter part of MIS (marine isotope stage) 10 (Figs. 3 and 4) (22). The amplitude of the glacial-interglacial variations in *G. ruber* $\delta^{18}\text{O}_{\text{calcite}}$ averages about 1.9‰, near the maximum for tropical Pacific cores (23, 24). The *G. ruber* Mg/Ca data indicate clear glacial-interglacial oscillations of 1 to 1.5 mmol/mol, with average values about 30% lower in glacial sections. Periodic changes in Mg/Ca always occur deeper in the core relative

to the oxygen isotopes, and they lead $\delta^{18}\text{O}_{\text{calcite}}$ by 5 to 10 cm or 2 to 4 thousand years (ky) (Figs. 3 and 4). Time-series analysis confirms that Mg/Ca leads $\delta^{18}\text{O}$ by 3 ky, indicating that the lead of SST over ice volume change must be at least 3 ky (25) [Web fig. 1 (26)]. The lead of SST over $\delta^{18}\text{O}$ has previously been observed in Southern Ocean (11, 27) and tropical Indian Ocean cores (28).

The SST change between the LGM and the core-top is $2.6 \pm 0.8^\circ\text{C}$ (Figs. 3 and 4 and Table 1). The maximum amplitude, observed between MIS 10 and MIS 9 onset and MIS 5.5 and MIS 4.2, is about 5°C. We confirmed the results for the youngest part of TR163-19 by determining Mg/Ca and $\delta^{18}\text{O}$ in *G. sacculifer* in TR163-19 and in *G. ruber* in a second core on the Cocos Ridge and two cores from the Galapagos Platform (Table 1) (29). These results agree within 0.5°C for the magnitude of glacial cooling in the EEP. Estimates of SST variability based on radiolaria microfossils from core RC13-110 (0°06'N, 86°29'W, 3231 m) lying just southwest of our study sites show similar temperature change (30).

The Mg/Ca records from three of the EEP cores indicate that early Holocene SST was ~1°C warmer than the core-tops, which have been dated to 950 to 1250 years before the present (yr B.P.) (31). The age of the SST maximum corresponds to the earliest Holocene. The SST maximum also corresponds to a similar feature in the Antarctic Vostok ice-core deuterium record (see below and Fig. 4) and the Huascarán ice core in Peru (9).

Western Pacific warm pool results from the Ontong Java Plateau. We analyzed $\delta^{18}\text{O}$ and Mg/Ca in *G. ruber* from the top 9.5 m of ODP Hole 806B on the OJP (Fig. 3) (32–34). The data indicate four complete glacial-interglacial oscillations back to MIS 12, at 450 ky B.P. The average $\delta^{18}\text{O}$ amplitude of the last two glacial-interglacial cycles is ~1.2‰, which is considerably smaller than the average value of 1.7‰ for moderate sedimentation rate deep-sea cores in the tropics (23). Previous studies have noted the generally smaller glacial-interglacial $\delta^{18}\text{O}$ amplitude in western Pacific cores relative to other basins and attributed it to unchanged glacial-interglacial SST, reduced amplitude due to bioturbation, and changes in surface salinity distribution (23, 24). The MIS 12-11 transition stands out with a much larger amplitude of almost 2‰, a feature which has previously been observed in several other cores from the OJP (35). The Mg/Ca data from Hole 806B indicate a glacial-interglacial amplitude of approximately 1 mmol/mol except on the MIS 12-11 and MIS 11-10 transitions, where the change is nearly 1.5 mmol/mol.

The changes in Hole 806B Mg/Ca, assuming a 9% increase in Mg/Ca per °C, equate to a $2.8^\circ \pm 0.7^\circ\text{C}$ drop in SST during the LGM and an average 3°C drop during glacial episodes (Fig. 3 and Table 1). The MIS 12-11 and MIS

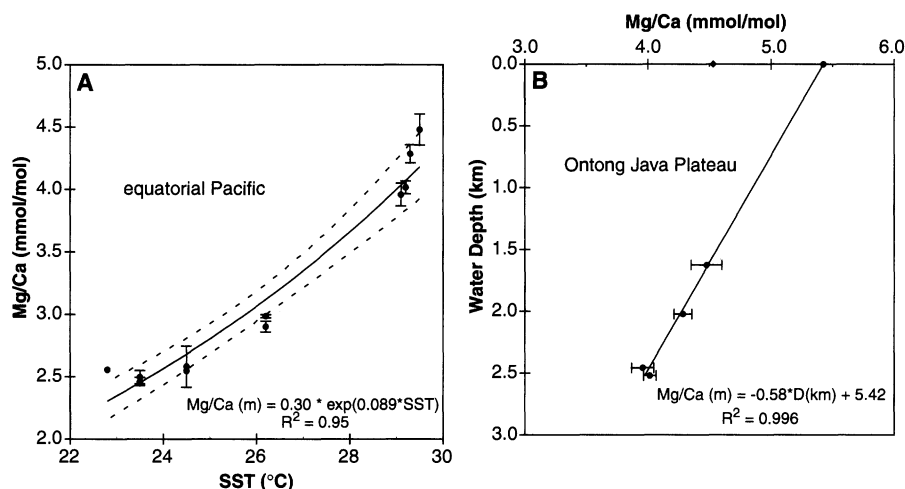


Fig. 2. (A) Pacific core-top *G. ruber* calibration for Mg/Ca versus mean annual SST (43). Each point is the average of two or more analyses. The range of core-top water depths is 1625 to 3200 m. The standard error of the exponential fit is $\pm 0.6^\circ\text{C}$. Dashed lines indicate the 95% confidence intervals for the curve fit. (B) Mg/Ca in *G. ruber* shells from core-tops on the Ontong Java Plateau as a function of water depth. The filled diamond at 0 m is the Mg/Ca value for a plankton tow sample taken at SST = 27.2°C off southwest Puerto Rico. The filled circle at 0 m is the same sample corrected for the 2°C warmer temperature of the WEP. The data indicate that shell Mg/Ca decreases by about 12% per 1 km increase in water depth. See text for details.

Table 1. Core locations, and core-top and last glacial maximum (LGM) data.

Core	Location (latitude, longitude, water depth)	Levitus SST (°C)	Mg/Ca (mmol/mol)		Core-top to LGM ΔSST^\dagger (°C)
			Core-top	LGM*	
TR 163-18	2°48.6'N, 89°51.1'W, 2030 m	26.2	3.15	2.39	-2.6 ± 0.7
TR 163-19	2°15.5'N, 90°57.1'W, 2348 m	26.2	2.99	2.38	-2.6 ± 0.8
TR 163-20B	0°47.3'N, 93°50.5'W, 3200 m	24.5	2.55	1.97	-2.9 ± 0.9
TR 163-22	0°30.9'N, 92°23.9'W, 2830 m	24.5	2.70	2.18	-2.4 ± 0.7
ODP 806B	0°19.1'N, 159°21.7'E, 2520 m	29.2	3.97	3.10	-2.8 ± 0.7

*Average of intervals corresponding to 18 to 24 ky B.P. †Calculated from the core-top and LGM Mg/Ca values and the *G. ruber* calibration in Fig. 2A. The estimated error of the core-top to LGM SST change is calculated from the deviation of core-top Mg/Ca-SST from Levitus SST (43), the standard deviation of the LGM Mg/Ca, and the standard error of the calibration (0.6°C). This error does not explicitly include the potential bias of downcore preservation changes, although preservation differences clearly contribute to the standard error of the calibration (Fig. 2).

11-10 transitions stand out with a 5°C change in SST. Spectral analysis demonstrates that maximum Mg/Ca leads minimum $\delta^{18}\text{O}$ by about 3 ky, as is seen for TR163-19 (36). We confirmed the *G. ruber* results for Hole 806B by measuring Mg/Ca and $\delta^{18}\text{O}$ in *G. sacculifer* for the youngest 60 ky of the core (37). We evaluated the potential influence of seafloor preservation changes by using the depth variation of sediments containing 80% CaCO_3 in the central equatorial Pacific over the last 470 ky (20) to estimate changes in lysocline depth [Web fig. 2 (26)]. The potential bias on SST estimates is +0.8°C for MIS 2 and MIS 3; in the rest of the record, the potential bias never exceeds $\pm 0.4^\circ\text{C}$. If these estimates of preservation are correct, they suggest that the actual SST decrease in the WEP during the LGM was $\sim 3.5^\circ\text{C}$.

SSTs for glacial MIS 2 and MIS 6 determined from OJP Hole 806B Mg/Ca data are $\sim 3^\circ\text{C}$ colder than modern values, compared to the 6°C cooling estimate determined from Sr/Ca of corals from the western tropical Pacific and dated to the Younger Dryas interval and termination II (6, 38). This difference is potentially reconciled by new evidence for glacial-interglacial changes in seawater Sr/Ca (39, 40). Foraminiferal Sr/Ca data in (40) suggest that seawater Sr/Ca during the LGM was $\sim 3\%$ higher than in the modern ocean [but see (39) for a different interpretation]. Because this difference is in the same direction as the average 5% higher Sr/Ca in glacial corals, when it is factored into the calculation of paleotemperatures, coral estimates actually indicate cooling of only 3°C (assuming 0.7% increase in coral Sr/Ca per °C lower SST), in agreement with the estimate based on Hole 806B Mg/Ca data.

The large amplitude change in $\delta^{18}\text{O}$ observed over MIS 12-11-10 in the Hole 806B record and other OJP sites (35) is matched by a similarly large amplitude signal in Mg/Ca (Fig. 3). Although Mg/Ca leads $\delta^{18}\text{O}$ by several ky, the large temperature change indicated by the Mg/Ca data must undoubtedly contribute to the coincidentally large $\delta^{18}\text{O}$ signal. Taken together, the Hole 806B $\delta^{18}\text{O}$ and Mg/Ca data indicate that MIS 11 and MIS 10 stand out as the warmest and coldest periods in the equatorial Pacific over the last 450 ky. SST extremes are 30°C for MIS 11 and 25°C for MIS 10, about 1°C warmer and colder, respectively, than averages for interglacial and glacial episodes. Previous studies have suggested that MIS 11 was a period of intense warmth and higher relative sea level, and faunal and isotopic records from the sub-Antarctic and North Atlantic indicate unusually warm conditions (27, 41). Sub-Antarctic cores also show enhanced cooling during MIS 10 and MIS 12 (27). Our data indicate that this climate amplification extended to the WEP.

Zonal gradients on the equator: comparison between the eastern and western Pacific. Temperature variability indicated by the Mg/Ca records show a strong correspondence be-

tween the eastern and western sites (Fig. 3). Some of the features that are clearly marked in the higher resolution TR163-19 record are not as apparent in the Hole 806B record, partly because of the presence of sampling gaps in Hole 806B. The poorest match occurs between 300 to 340 ky (MIS 9), which we attribute to uncertainty in the stratigraphy for ODP 806B in this interval because of a disturbed coring interval at 6.5 to 6.9 m (~ 308 to 327 ky) (42). These sites suggest a consistent picture of about 3° to 4°C colder equatorial Pacific SST during glacial episodes.

The mean SST difference between the WEP and EEP sites is $2.8^\circ \pm 0.8^\circ\text{C}$ (averaged over a time step of 2 ky), compared to a modern mean annual SST difference of 3°C (43). The zonal gradient appears to be $\sim 1^\circ\text{C}$ larger than the

mean value during glacial episodes (e.g., MIS 2, 6, 8) and $\sim 1^\circ\text{C}$ smaller during the warmest interglacial periods (e.g., MIS 5.5, 7.5, 9.3) (Fig. 3). This observation is supported by faunal studies indicating an increase in the Pacific zonal thermocline gradient during the LGM (44). The inferred changes in the zonal SST gradient might reflect enhanced trade winds during glacial episodes, analogous to the La Niña state of the modern Pacific.

Why is the glacial-interglacial $\delta^{18}\text{O}$ amplitude in the WEP so much smaller than its counterpart in the EEP? Temperature changes implied by the Mg/Ca data are similar in the EEP and WEP (Fig. 3). The similar magnitude of Mg/Ca change at the two sites rules out bioturbation as the cause, although it could certainly account for a reduction of amplitude in

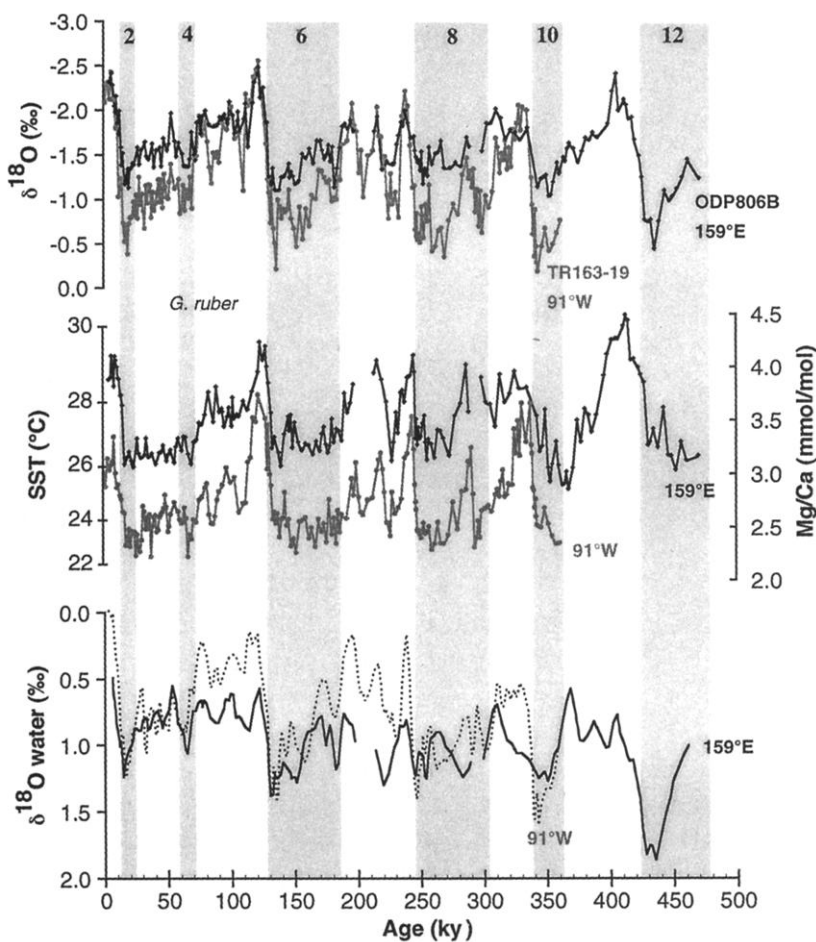


Fig. 3. Equatorial Pacific records from Cocos Ridge core TR163-19 (90°57'W, 2°16'N, 2348 m) and Ontong Java Plateau core ODP Hole 806B (159°22'E, 0°19'N, 2520 m), based on the surface-dwelling planktonic foraminifera *G. ruber*. The age scale is based on radiocarbon dates for the core-tops and the SPECMAP age scale (53). Gaps in the Hole 806B record are due to coring and sampling gaps. Each Mg/Ca point is the average of two analyses. The SST scale for Mg/Ca is nonlinear and is based on conversion of Mg/Ca data using the relationship: $\text{SST } (^\circ\text{C}) = 0.089^{-1} \cdot \ln[\text{Mg/Ca (m)}/0.3]$. The lower panel depicts $\delta^{18}\text{O}_w$ (SMOW, standard mean ocean water scale) calculated from the $\delta^{18}\text{O}$ and temperature estimates using a paleotemperature equation (45, 46). The $\delta^{18}\text{O}_w$ data has been smoothed with a triangular digital filter for clarity. The estimated confidence interval for the $\delta^{18}\text{O}_w$ estimates is $\pm 0.18\text{‰}$. Modern SST, sea-surface salinity, and $\delta^{18}\text{O}_w$ estimates for the sites are: 29.2°C, 34.6 practical salinity unit (PSU), and 0.3‰, respectively, for the OJP and 26.2°C, 33.4 PSU, and -0.1‰ for the Cocos Ridge (43, 47–49). The numbered, shaded bars indicate marine isotope stages.

both geochemical signals. These observations in turn suggest that the only viable explanation for the smaller $\delta^{18}\text{O}$ amplitude at site 806B is a shift in the equatorial Pacific zonal $\delta^{18}\text{O}_w$ (salinity) gradient during glacial episodes.

By combining the Mg/Ca-based SST estimates with measured $\delta^{18}\text{O}$, we calculated $\delta^{18}\text{O}_w$ values for the two long records in this study (Fig. 3) (45, 46). Calculated $\delta^{18}\text{O}_w$ values for the core-tops are 0.5‰ for the OJP and

0‰ for the Cocos Ridge, in agreement with the modern inferred $\delta^{18}\text{O}_w$ values of 0.3‰ and -0.1‰ for the sites, calculated from the salinity of the overlying waters and regional $\delta^{18}\text{O}_w$ -S relationships (47–49). At the EEP site (TR163-19), the average glacial-interglacial $\delta^{18}\text{O}_w$ amplitude is 1.2‰, close to previous estimates of the change in mean ocean $\delta^{18}\text{O}_w$ due to changing ice volume (50). At the WEP site (ODP 806B), the average glacial-interglacial amplitude of $\delta^{18}\text{O}_w$ is only 0.7‰ back to MIS 11. This difference is a consequence of similar Mg/Ca-based SST signals accompanying very different $\delta^{18}\text{O}$ -calcite amplitudes.

Taking the results for $\delta^{18}\text{O}_w$ at face value suggests that the zonal $\delta^{18}\text{O}_w$ gradient between the eastern and western Pacific decreased during glacial episodes. These data reveal a recurring pattern of similar $\delta^{18}\text{O}_w$ values during glacial intervals (i.e., MIS 4-2, MIS 6, MIS 8) and offset values during interglacial intervals (i.e., MIS 1, MIS 5, MIS 7, MIS 9). The observation that the EEP site experienced a glacial-interglacial $\delta^{18}\text{O}_w$ change consistent with estimates of the change due to ice volume implies that $\delta^{18}\text{O}_w$ (and salinity) decreased in the WEP relative to the global ocean value. A decrease in WEP salinity (of ~1 PSU or more) would also increase the overall Atlantic-Pacific salinity contrast during glacial episodes, as previously suggested on the basis of oxygen isotope data alone (51). One potential mechanism for these changes is an increase in precipitation in the WEP analogous to the La Niña state of the modern Pacific, perhaps connected to enhanced westerly transport of water vapor by stronger glacial trade winds (44). This explanation is supported by increased Pacific zonal SST gradients during glacial episodes (Fig. 3).

The calculated $\delta^{18}\text{O}_w$ records from both sites reveal a secular increase in $\delta^{18}\text{O}_w$ with age, with a slope of +0.1‰ per 100 ky. This secular increase in $\delta^{18}\text{O}_w$ is apparent in the foraminifer shell $\delta^{18}\text{O}$ data from the two cores as well as other planktic oxygen isotope records from the Pacific (35), and it might be part of a longer cycle such as the 400-ky orbital cycle. The longer record from ODP Hole 806B reveals a large-scale change in $\delta^{18}\text{O}_w$ in MIS 10-12. A $\delta^{18}\text{O}_w$ record from the northeast Atlantic based on benthic $\delta^{18}\text{O}$ and assumptions about deep-ocean cooling reveal a similar event, with a large positive excursion centered on 430 ky, just as is observed in the Hole 806B $\delta^{18}\text{O}_w$ record (41). The coincidence of these features suggests a global signal that is likely to have its origins in either a greater drop in sea level during MIS 12 and/or deposition of more isotopically depleted continental ice.

Global synchrony and implications for climate evolution. The lead of temperature over $\delta^{18}\text{O}$ observed in the Cocos Ridge core provides a potential solution to a long-standing controversy in paleoclimatology. The Devils Hole $\delta^{18}\text{O}$ record from a vein calcite precipi-

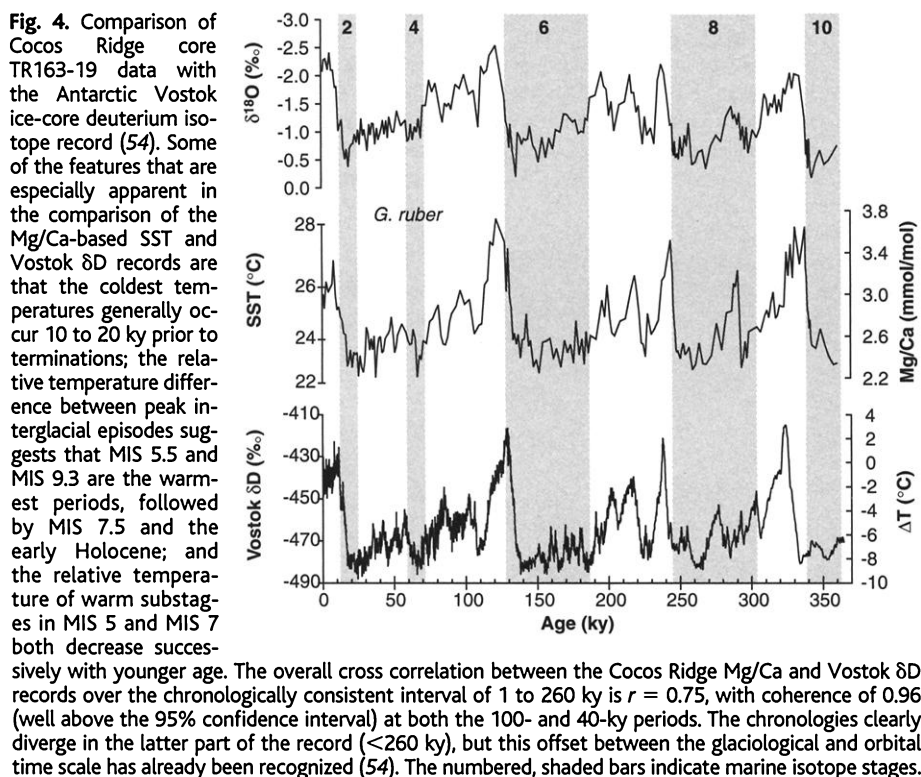


Fig. 4. Comparison of Cocos Ridge core TR163-19 data with the Antarctic Vostok ice-core deuterium isotope record (54). Some of the features that are especially apparent in the comparison of the Mg/Ca-based SST and Vostok δD records are that the coldest temperatures generally occur 10 to 20 ky prior to terminations; the relative temperature difference between peak interglacial episodes suggests that MIS 5.5 and MIS 9.3 are the warmest periods, followed by MIS 7.5 and the early Holocene; and the relative temperature of warm substages in MIS 5 and MIS 7 both decrease successively with younger age. The overall cross correlation between the Cocos Ridge Mg/Ca and Vostok δD records over the chronologically consistent interval of 1 to 260 ky is $r = 0.75$, with coherence of 0.96 (well above the 95% confidence interval) at both the 100- and 40-ky periods. The chronologies clearly diverge in the latter part of the record (<260 ky), but this offset between the glaciological and orbital time scale has already been recognized (54). The numbered, shaded bars indicate marine isotope stages.

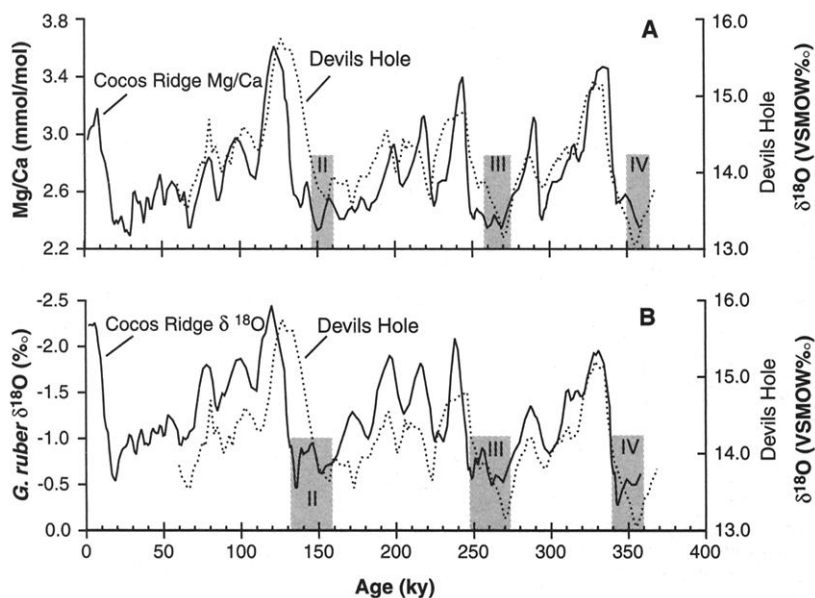


Fig. 5. Comparison of TR163-19 Mg/Ca (A) and $\delta^{18}\text{O}$ (B) records (digitally smoothed with a triangular filter to remove higher frequency components) and the Devils Hole $\delta^{18}\text{O}$ record (52). The chronology for the Cocos Ridge records is based on the SPECMAP orbital time scale (53). The Devils Hole record is on a time scale derived from U-Th disequilibrium dating (52). The beginning of glacial terminations is indicated by the gray bars. In the Cocos Ridge Mg/Ca–Devils Hole comparison, the beginning of warming at terminations is coincident within 0 to 5 ky. The correlation is $r = 0.73$ with 0 phase lag. In the Cocos Ridge $\delta^{18}\text{O}$ –Devils Hole comparison, Devils Hole consistently begins to warm 10 to 20 ky earlier. The correlation is $r = 0.61$ with the Cocos Ridge record lagging by 5 ky. VSMOW, Vienna standard mean ocean water.

tated in a groundwater-submerged fissure in the Great Basin (Nevada) and independently dated by U disequilibrium series, indicates large glacial-interglacial oscillations that lead foraminiferal $\delta^{18}\text{O}$ records by up to 20 ky (52). Initial publications describing this lead questioned the veracity of the entire orbitally tuned SPECMAP time scale, which is fundamental to Milankovitch theory (53). The lead in Mg/Ca-based temperatures over $\delta^{18}\text{O}$ in our records suggests that if the Devils Hole data records temperature change, it should be in phase with oceanic temperature records but lead oceanic ice volume records.

A comparison of the EEP Cocos Ridge Mg/Ca record (TR163-19) and the Devils Hole record, each on completely independent chronologies (Fig. 5A), indicates that the two records are in phase and match significantly better than is observed for the foraminiferal $\delta^{18}\text{O}$ comparison (Fig. 5B) [Web fig. 3 (26)]. Comparison of the beginning of terminations II, III, and IV in the Mg/Ca and Devils Hole implies synchronous warming within 3 ky. The same comparison for the Cocos Ridge $\delta^{18}\text{O}$ and Devils Hole record confirms the previously recognized lead of Devils Hole. The simplest explanation for the overall in-phase correspondence between Cocos Ridge Mg/Ca and Devils Hole $\delta^{18}\text{O}$ is that SST changes in the eastern Pacific are transmitted via the moisture carried by the westerlies to the western interior of North America.

Further evidence of connections between the tropical Pacific and global climate comes from comparison of the Cocos Ridge records with the Antarctic Vostok ice-core deuterium record (54). Many features can be traced between the Cocos Ridge Mg/Ca and Vostok δD temperature records, one on the equator and one near the South Pole (Fig. 4). The correspondence between the two records indicates synchronous (within the 2-ky resolution of the sites) global temperature change in the Antarctic atmosphere and EEP surface ocean. The magnitude of the inferred temperature changes is approximately double for air temperature over Vostok, consistent with the greater sensitivity of polar regions and the lower heat capacity of the atmosphere and in agreement with a previous comparison of sub-Antarctic SST records and Vostok-inferred air temperatures that also reveal a greater magnitude for air temperature changes (11).

Our results demonstrate that equatorial Pacific SST was about 3°C colder than modern conditions during glacial episodes of the last 500 ky, and that the western Pacific warm pool, the oceanic region most isolated from continental ice sheets (3), was a dynamic part of glacial-interglacial climate change. The timing of SST change precedes the formation and demise of continental ice sheets by at least 3 ky. Similar results from other tropical sites in the Atlantic and Indian Oceans (12, 28) suggest that tropical surface water cooling was a synchronous glo-

bal-scale feature. Tropical Pacific cooling is certain to have played a major role in forcing climate change both directly through heat exchange with the atmosphere and indirectly through its impact on the water and CO_2 content of the atmosphere.

References and Notes

- M. A. Cane, *Science* **282**, 59 (1998).
- CLIMAP, *Geol. Soc. Am. Map Chart Ser. MC-36* (1981).
- T. J. Crowley, *Clim. Dyn.* **16**, 241 (2000).
- M. W. Lyle, F. G. Prahl, M. A. Sparrow, *Nature* **355**, 812 (1992).
- C. Pelejero, J. O. Grimalt, S. Heilig, M. Kienast, L. Wang, *Paleoceanography* **14**, 224 (1999).
- J. W. Beck, J. Recy, F. Taylor, R. L. Edwards, G. Cabloh, *Nature* **385**, 705 (1997).
- D. Rind and D. Peteet, *Quat. Res.* **24**, 1 (1985).
- M. Stute et al., *Science* **269**, 379 (1995).
- L. G. Thompson et al., *Science* **269**, 46 (1995).
- D. W. Hastings, A. D. Russell, S. R. Emerson, *Paleoceanography* **13**, 161 (1998).
- T. A. Mashiotta, D. W. Lea, H. J. Spero, *Earth Planet. Sci. Lett.* **170**, 417 (1999).
- D. Nürnberg, A. Müller, R. R. Schneider, *Paleoceanography* **15**, 124 (2000).
- H. Elderfield and G. Ganssen, *Nature* **405**, 442 (2000).
- D. Nürnberg, J. Bijma, C. Hemleben, *Geochim. Cosmochim. Acta* **60**, 803 (1996).
- D. W. Lea, T. A. Mashiotta, H. J. Spero, *Geochim. Cosmochim. Acta* **63**, 2369 (1999).
- Methods: For Mg/Ca, about 50 to 60 *Globigerinoides* shells were picked from the 250- to 350- μm fraction of the cores, of which 10 to 15 shells were separated for isotopic analysis (see below). The remaining shells, weighing about 0.6 mg, were gently crushed open and split into two aliquots that were cleaned of contaminating phases using a multi-step cleaning procedure developed for trace element analysis. Splits of the sample were analyzed in separate runs and results compared to judge overall reproducibility (see below). Cleaning tests on Holocene and glacial samples from TR163-19 reveal a small but significant decrease in Mg/Ca with more intense cleaning, and an apparent improvement in reproducibility of sample splits. Samples were simultaneously dissolved and analyzed by isotope dilution inductively coupled plasma mass spectrometry (17). Long-term reproducibility of Mg/Ca determinations is estimated at $\pm 2.1\%$ (1σ) based on 268 analyses of consistency standard CN3 (Mg/Ca = 1.56 ± 0.03 mmol/mol), matched in Ca concentration to the average foraminifer sample, and analyzed over a 2-year period with the samples that were used in this study. The average reproducibility of sample splits from sediment intervals in TR163-19 and ODP806B was ± 0.08 and ± 0.09 mmol/mol, respectively, equivalent to $\pm 3\%$ and $\pm 2.4\%$, respectively. For analysis of $\delta^{18}\text{O}$ in foraminiferal calcite, between 10 to 15 shells were pooled, sonicated for 5 s in methanol, and roasted at 375°C for 30 min in vacuo, then reacted individually in 105% H_3PO_4 at 90°C using an Isocarb common acid bath autocarbonate device. The resulting CO_2 was then analyzed by a Fisons Optima isotope ratio mass spectrometer. Data are presented in standard delta notation as the per mil (‰) difference from the Pee Dee Belemnite (PDB) standard. The analytical precision of the measurements is better than $\pm 0.06\%$, as determined by replicate analyses of NIST-19 and a second Carrara marble laboratory standard.
- D. W. Lea and P. A. Martin, *Geochim. Cosmochim. Acta* **60**, 3143 (1996).
- Y. Rosenthal, G. P. Lohmann, K. C. Lohmann, R. M. Sherrell, *Paleoceanography* **15**, 135 (2000).
- J. Le and N. J. Shackleton, *Paleoceanography* **7**, 21 (1992).
- J. W. Farrell and W. L. Prell, *Paleoceanography* **4**, 447 (1989).
- Numerous studies, including many on OJP sediments, have demonstrated that preservation in the equatorial Pacific is favored during glacial episodes (19, 20). Based on dissolution indices, peak preservation on the OJP appears to lag peak glaciation by 6 to 20 ky (19). Our core-top results from the OJP demonstrate that increasing preservation leads to higher shell Mg/Ca, presumably because more ontogenetic calcite is present. Therefore, increased preservation during glacial intervals would tend to bias shell Mg/Ca to higher values, opposite to the observed signal, which would therefore reduce the amplitude of Mg/Ca cycles. Given an estimated deepening by 300 to 600 m of the lysocline during glacial episodes (20) and the observed 12% decrease in shell Mg/Ca per kilometer water depth, we estimate that shell Mg/Ca during glacial intervals might be increased by about 5% by enhanced preservation, which is equivalent to about 0.5°C.
- The sites in the eastern tropical Pacific are TR163-18 and TR163-19 on the southwest Cocos Ridge and TR163-20B and TR163-22 on the Galapagos Platform (Table 1). TR163-18 and TR163-19 lie in the warmer province of the North Equatorial Counter Current on the Cocos Ridge and TR163-20B and TR163-22 lie in the cooler province of the South Equatorial Current on the Galapagos Platform. Accelerator mass spectrometry radiocarbon ages for *Neogloboquadrina dutertrei* shells from the core-tops range between 1570 to 3460 years (uncorrected), relatively young for Pacific core-tops. Sedimentation rates, as determined from the chronologies developed from the isotopic stratigraphy, range from ~ 3 cm/ky for cores TR163-18, TR163-19, and TR163-20B to up to 10 cm/ky for TR163-22. Core depths (2030 to 3200 m) are all shallower than the regional lysocline, estimated at 4 km. Despite the shallow depth, foraminifer shells appear to have undergone at least some fragmentation and dissolution in the interglacial sections of this core. Chronologies for the TR163 cores are based on planktonic oxygen isotope records correlated to the standard SPECMAP chronology and core-top radiocarbon ages. All of the oxygen isotope substages are present in TR163-19 (Fig. 3), allowing development of an age scale based on 38 points. TR163-19 was sampled at 5-cm intervals, equivalent to a potential resolution of about 2 ky.
- W. S. Broecker, *Quat. Res.* **26**, 121 (1986).
- J. I. Martinez, P. De Deckker, A. R. Chivas, *Mar. Micropaleontol.* **32**, 311 (1997).
- The overall correlation between Mg/Ca and $\delta^{18}\text{O}$ is $r = -0.84$ with Mg/Ca leading by 3 ky. Spectral variance in the TR163-19 records is concentrated at the major orbital periods of 100, 41, and 23 ky. The coherence between the two records at these periods is 0.98, 0.99, and 0.99 respectively, all of which readily exceed the coherence test statistic for 95% CI, which is 0.83. Mg/Ca leads at all three periods, by 9 ± 2 , 3 ± 1 , and 1.6 ± 0.6 ky, respectively.
- Supplementary material is available at www.sciencemag.org/feature/data/1050876.sml
- J. D. Hays, J. Imbrie, N. J. Shackleton, *Science* **194**, 1121 (1976).
- E. Bard, F. Rostek, C. Sonzogni, *Nature* **385**, 707 (1997).
- We verified the youngest part of the *G. ruber* record in TR163-19 by measuring Mg/Ca and $\delta^{18}\text{O}$ in *G. sacculifer* shells. The trends between the species are consistent, but there is a considerable offset in the Mg/Ca values, with *G. ruber* shells consistently higher by ~ 0.5 mmol/mol, equivalent to about 2°C. This offset is also seen in the $\delta^{18}\text{O}$ values for the two species, with *G. sacculifer* $\delta^{18}\text{O}$ averaging 1‰ more positive. These offsets most likely reflect the (greater) addition of gametogenic calcite to *G. sacculifer*, estimated to be as high as 30% of the total shell mass for this species, added at cold thermocline temperatures (18). The Mg/Ca change in *G. sacculifer* over termination I is 2.06 to 2.55 mmol/mol, equivalent to $+2.4^\circ\text{C}$ and within error of the estimate based on *G. ruber*.
- N. G. Pisias and A. C. Mix, *Paleoceanography* **12**, 381 (1997).
- The three cores that show this feature and their core-top radiocarbon ages are: TR163-19, 1040 years B.P.; TR163-20B, 1250 years B.P.; and, TR163-22, 950 years B.P. These ages are reservoir-corrected by 620 years.
- W. H. Berger, T. Bickert, H. Schmidt, G. Wefer, in *Proc. Ocean Drill. Program Sci. Results*, W. H. Berger et al., Eds. (Ocean Drilling Program, College Station, TX, 1993), vol. 130, pp. 381-395.
- The study site on the Ontong Java Plateau (OJP) is Ocean Drilling Program (ODP) Hole 806B. The site lies at 2520 m, considerably shallower than the regional lysocline at 3400 m and the calcite saturation horizon

- at 3 km. The $\delta^{18}\text{O}$ record for *G. ruber* is very similar to the previously published record for *G. sacculifer* from 806B, as well as other piston cores from the OJP, but our sampling resolution is twice that of the previous study of Hole 806B. We slightly modified the existing age model using our *G. ruber* $\delta^{18}\text{O}$ record, generated at twice the resolution, correlated to the standard SPEC-MAP chronology. We also corrected the core-top age to the typical radiocarbon age of core-tops from this region and depth (34). The average sedimentation rate is about 2 cm/ky.
34. W. S. Broecker, E. Clark, D. C. McCorkle, I. Hajdas, G. Bonani, *Paleoceanography* **14**, 13 (1999).
 35. N. J. Shackleton, J. Le, A. Mix, M. A. Hall, *Quat. Sci. Rev.* **11**, 387 (1992).
 36. Spectral analysis of Hole 806B data indicates that the overall cross correlation between Mg/Ca and $\delta^{18}\text{O}$ is $r = -0.73$, with Mg/Ca leading by 3 ky. The 100-, 41-, and 23-ky orbital periods in the $\delta^{18}\text{O}$ and Mg/Ca records are all coherent at the 95% Cl.
 37. We determined $\delta^{18}\text{O}$ and Mg/Ca in *G. sacculifer* shells from the top 150 cm of Hole 806B. As is observed for TR163-19, the Mg/Ca values for *G. sacculifer* are systematically lower than for *G. ruber* and the $\delta^{18}\text{O}$ values are systematically more positive. The *G. sacculifer* Mg/Ca change over termination I is 2.8 to 3.6 mmol/mol, equivalent to a 2.8°C increase in SST and essentially identical to the SST change calculated from the *G. ruber* data.
 38. M. T. McCulloch et al., *Science* **283**, 202 (1999).
 39. H. M. Stoll, D. P. Schrag, S. C. Clemens, *Geochim. Cosmochim. Acta* **63**, 3535 (1999).
 40. P. A. Martin, D. W. Lea, T. A. Mashiotta, T. Papenfuss, M. Sarnthein, *Geochem. Geophys. Geosyst.* **1**, Paper Number 1999GC000006 (1999).
 41. J. F. McManus, D. W. Oppo, J. L. Cullen, *Science* **283**, 971 (1999).
 42. L. W. Kroenke et al., *Proc. Ocean Drill. Program*, E. M. Barbu, Ed. (Ocean Drilling Program, College Station, TX, 1991), vol. 130.
 43. S. Levitus and T. P. Boyer, *World Ocean Atlas 1994, Volume 4: Temperature*, NOAA Atlas NESDIS (U.S. Department of Commerce, Washington, DC, 1994). Accessed at <http://ingrid.ldgo.columbia.edu/SOURCES/LEVITUS94/>
 44. D. J. Andreasen and A. C. Ravelo, *Paleoceanography* **12**, 395 (1997).
 45. We used a low-light paleotemperature equation derived for *Orbulina universa* (46): $\delta^{18}\text{O}_w = (T - 16.5 + 4.8 * \delta^{18}\text{O}_{\text{calcite}}) / 4.8 + 0.27$. Because the slopes of $\delta^{18}\text{O}$ change versus temperature are similar (0.20 to 0.23‰ per °C), the choice of paleotemperature equations does not have a large impact on the calculations. The estimated uncertainty of the $\delta^{18}\text{O}_w$ values is $\pm 0.18\text{‰}$, calculated from the uncertainty in the paleotemperature equation, the standard error of the Mg/Ca-SST calibration, and the reproducibility of $\delta^{18}\text{O}$ and Mg/Ca in a typical interval.
 46. B. E. Bemis, H. J. Spero, J. Bijma, D. W. Lea, *Paleoceanography* **13**, 150 (1998).
 47. S. Levitus, R. Burgett, T. P. Boyer, *World Ocean Atlas 1994, Volume 3: Salinity*, NOAA Atlas NESDIS (U.S. Department of Commerce, Washington, D.C., 1994). Accessed at <http://ingrid.ldgo.columbia.edu/SOURCES/LEVITUS94/>
 48. R. G. Fairbanks et al., *Coral Reefs* **16**, S93 (1997).
 49. R. G. Fairbanks, M. Sverdløve, R. Free, P. H. Wiebe, A. W. H. Bé, *Nature* **298**, 841 (1982).
 50. D. P. Schrag, G. Hampt, D. W. Murray, *Science* **272**, 1930 (1996).
 51. W. S. Broecker, *Paleoceanography* **4**, 207 (1989).
 52. I. J. Winograd et al., *Science* **258**, 255 (1992).
 53. J. Imbrie et al., in *Milankovitch and Climate, Part 1*, A. L. Berger, J. Imbrie, J. Hays, G. Kukla, B. Saltzman, Eds. (Reidel, Dordrecht, Netherlands, 1984), pp. 269–305.
 54. J. R. Petit et al., *Nature* **399**, 429 (1999).
 55. We thank J. Kennett and D. McCorkle for samples; T. Crowley, E. Bard, H. Elderfield, N. Pisis, and P. Martin for comments on earlier drafts; M. Kashgarian and T. Guilderson for radiocarbon dating; P. Howell for time-series software and advice on its use; I. Winograd for the suggestion to compare to the Devils Hole record; Q. Xie, G. Paradis, and H. Berg for mass spectrometer operation and maintenance; D. Gates, A. Schilla, P. Dekens, A. Davé, P. von Langen, L. Juranek, and M. Thomas for sample preparation; and E. Christian for clerical assistance. This research was funded by the NSF.

29 March 2000; accepted 13 July 2000

Molecular Evidence for the Early Evolution of Photosynthesis

Jin Xiong,¹ William M. Fischer,¹ Kazuhito Inoue,² Masaaki Nakahara,² Carl E. Bauer^{1*}

The origin and evolution of photosynthesis have long remained enigmatic due to a lack of sequence information of photosynthesis genes across the entire photosynthetic domain. To probe early evolutionary history of photosynthesis, we obtained new sequence information of a number of photosynthesis genes from the green sulfur bacterium *Chlorobium tepidum* and the green nonsulfur bacterium *Chloroflexus aurantiacus*. A total of 31 open reading frames that encode enzymes involved in bacteriochlorophyll/porphyrin biosynthesis, carotenoid biosynthesis, and photosynthetic electron transfer were identified in about 100 kilobase pairs of genomic sequence. Phylogenetic analyses of multiple magnesium-tetrapyrrole biosynthesis genes using a combination of distance, maximum parsimony, and maximum likelihood methods indicate that heliobacteria are closest to the last common ancestor of all oxygenic photosynthetic lineages and that green sulfur bacteria and green nonsulfur bacteria are each other's closest relatives. Parsimony and distance analyses further identify purple bacteria as the earliest emerging photosynthetic lineage. These results challenge previous conclusions based on 16S ribosomal RNA and Hsp60/Hsp70 analyses that green nonsulfur bacteria or heliobacteria are the earliest phototrophs. The overall consensus of our phylogenetic analysis, that bacteriochlorophyll biosynthesis evolved before chlorophyll biosynthesis, also argues against the long-held Granick hypothesis.

The advent of photosynthesis is one of the central events in the early development of life on Earth. The origin and evolution of photo-

synthesis, however, have long remained unresolved. Studies have demonstrated that photosynthetic eukaryotes acquired photosynthetic properties from endosymbiosis with cyanobacteria (1). This observation, coupled with the fact that no Mg-tetrapyrrole-based photosynthesis has been found in Archaea, supports the notion that photosynthesis is a bacterially derived process (2). To obtain insight into the early evolution of photosynthe-

sis, it is essential to conduct detailed phylogenetic analysis of many photosynthesis genes from each of the five known photosynthetic bacterial lineages. However, a paucity of photosynthesis gene sequences across the entire spectrum of photosynthetic bacteria has required that previous analyses rely on the use of nonphotosynthesis genes, which have given conflicting results for the evolution of photosynthesis and of photosynthetic organisms. For example, phylogenetic analysis of small-subunit rRNA suggests that green nonsulfur bacteria are the earliest evolving photosynthetic lineage (3). In contrast, using portions of the Hsp60 and Hsp70 heat shock proteins as markers, Gupta et al. (4) concluded that heliobacteria are the earliest evolving photosynthetic lineage and that this lineage subsequently diverged to green nonsulfur bacteria, cyanobacteria, green sulfur bacteria, and purple bacteria, in that order. The conflicting trees derived from such studies indicate that extrapolating the evolution of photosynthesis from nonphotosynthesis gene trees may be invalid.

Another problem arises when only a single set of photosynthesis genes is used for phylogeny. Previous attempts to analyze the evolution of photosynthesis using photosynthetic reaction center apoproteins failed to construct a phylogeny that includes all five photosynthetic bacterial lineages, because anoxygenic photosynthetic bacteria contain only one type of photosynthetic reaction center (type I or type II), whereas cyanobacteria contain both types of reaction center. Though the two types of reaction centers share significant structural similarities (5), their sequences have diverged to such an extent that it is virtually impossible to perform a statistically

¹Department of Biology, Indiana University, Bloomington, IN 47405, USA. ²Department of Biological Sciences, Kanagawa University, Hiratsuka, Kanagawa, 259-1293, Japan.

*To whom correspondence should be addressed. E-mail: cbauer@bio.indiana.edu